

**Electronic Supplementary information (ESI) for**  
**High-Performance Electrothermal and Anticorrosive Transparent**  
**Heating Stickers**

*Kangmin Lee,<sup>a‡</sup> Jeonghwan Park,<sup>ac‡</sup> Hyungwoo Kim,<sup>a</sup> Han-Saem Park,<sup>a</sup> Hyun-Kon Song,<sup>a</sup> Ka-  
Hyun Kim,<sup>\*b</sup> and Kwanyong Seo<sup>\*a</sup>*

<sup>a</sup> Department of Energy Engineering, Ulsan National Institute of Science and Technology  
(UNIST), Ulsan 44919, Republic of Korea

<sup>b</sup>KIER-UNIST, Advanced Center for Energy Korea Institute for Energy Research, Ulsan 44919,  
Republic of Korea

<sup>c</sup> Department of Physics, Center for Attosecond Science and Technology Pohang University of  
Science and Technology and Max Planck POSTECH/KOREA Res. Init., Pohang, Gyeongbuk  
37673, Republic of Korea

‡ These authors contributed equally to this work

\*Corresponding authors. E-mail: ka-hyun.kim@kier.re.kr, kseo@unist.ac.kr

## SUPPORTING FIGURES

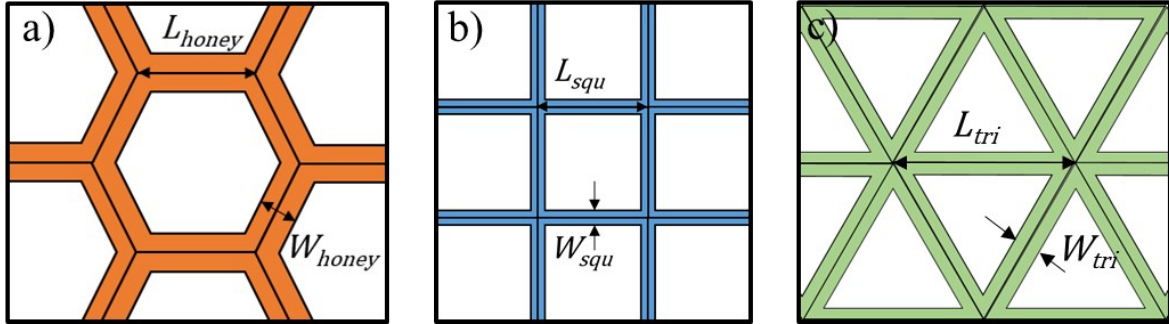


**Fig. S1.** Schematic of a) hexagonal, b) square, and c) triangular grid pattern.

We have modeled three types of grid pattern, the honeycomb, square, and triangle with the same transmittance and same volume of empty space enclosed by a grid in Solidworks flow simulation (Figure S1a–c).

### 1. Same transmittance

First, we set the conditions of each grid pattern so that their transmittance was the same. The transmittance represents the ratio of the total area to that of the empty space (without the grid area). Therefore, the transmittance can be expressed by the following equation:

- Transmittance of honeycomb grid pattern:  $T_{honey}(\%) = \left(1 - \frac{W_{honey}}{\sqrt{3}L_{honey}}\right)^2 \times 100(\%)\dots\textcircled{1}$

- Transmittance of square grid pattern:  $T_{squ}(\%) = \left(1 - \frac{W_{squ}}{L_{squ}}\right)^2 \times 100(\%)\dots\textcircled{2}$

- Transmittance of triangular grid pattern:  $T_{tri}(\%) = \left(1 - \frac{\sqrt{3}W_{tri}}{L_{tri}}\right)^2 \times 100(\%)\dots\textcircled{3}$ ,

where  $T$ ,  $W$ , and  $L$  represent the transmittance, width, and length of the grid pattern, respectively. When the transmittance of each grid pattern is the same ( $T_{honey} = T_{squ} = T_{tri}$ ), equation ①, ②, and ③ can be represented as follows:

$$\left(1 - \frac{W_{honey}}{\sqrt{3}L_{honey}}\right)^2 \times 100(\%) = \left(1 - \frac{W_{squ}}{L_{squ}}\right)^2 \times 100(\%) = \left(1 - \frac{\sqrt{3}W_{tri}}{L_{tri}}\right)^2 \times 100(\%).$$

This equation is simplified as follows:

$$\frac{W_{honey}}{\sqrt{3}L_{honey}} = \frac{W_{squ}}{L_{squ}} = \frac{\sqrt{3}W_{tri}}{L_{tri}} \dots \text{④}.$$

We can then obtain the relation between the width ( $W$ ) and length ( $L$ ) of each grid pattern.

## 2. Same volume of empty space

Secondly, we have modeled each grid pattern to have the same volume of empty space. The volume of empty space can be calculated by multiplying the thickness of the grid by the area of empty space. Accordingly, this can be written as follows:

- Volume of empty space in honeycomb grid pattern:  $V_{honey} = \frac{3\sqrt{3}}{2}t(L_{honey} - \frac{W_{honey}}{\sqrt{3}})^2 \dots \text{⑤}.$

- Volume of empty space in square grid pattern:  $V_{squ} = t(L_{squ} - W_{squ})^2 \dots \text{⑥}.$

- Volume of empty space in triangular grid pattern:  $V_{tri} = \frac{\sqrt{3}}{4}t(L_{tri} - \sqrt{3}W_{tri})^2 \dots \text{⑦}.$

Where  $V$ ,  $t$ , and  $L$  represent the volume of empty space, thickness of the grid pattern, and length of the grid pattern, respectively.

It is assumed that the grid patterns have the same thickness. When the grid patterns have the same volume of empty space ( $V_{honey} = V_{squ} = V_{tri}$ ), equation ⑤, ⑥, and ⑦ can be represented as follows:

$$(L_{honey} - \frac{W_{honey}}{\sqrt{3}})^2 = \frac{2}{3\sqrt{3}}(L_{squ} - W_{squ})^2 = \frac{1}{6}(L_{tri} - \sqrt{3}W_{tri})^2 \dots \textcircled{8}.$$

From equation ④ and ⑧, we can obtain the relation between the length ( $L$ ) and width ( $W$ ) of each grid pattern as follows:

$$L_{honey}^2 = \frac{2}{3\sqrt{3}}L_{squ}^2 = \frac{1}{6}L_{tri}^2 \dots \textcircled{9},$$

$$W_{honey}^2 = \frac{2}{\sqrt{3}}W_{squ}^2 = \frac{3}{2}W_{tri}^2 \dots \textcircled{10}.$$

After modeling each grid pattern to satisfy equation ⑨ and ⑩, we simulated the heat flow of each grid pattern to have the same amount of heat per unit volume of grid ( $W m^{-3}$ ). We can thus confirm that the heat was distributed as shown in Movie S1–3 (Supporting Information). These confirm that heat distribution in the honeycomb pattern was 1.35 and 2.1 times faster than in the triangle and square, respectively.

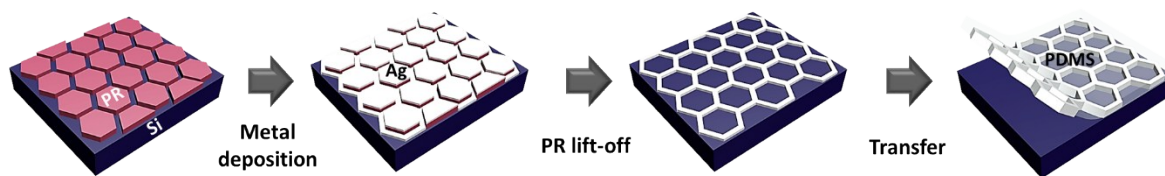


**Fig. S2.** Schematic of the fabrication of Ag microgrid electrodes embedded in PDMS.

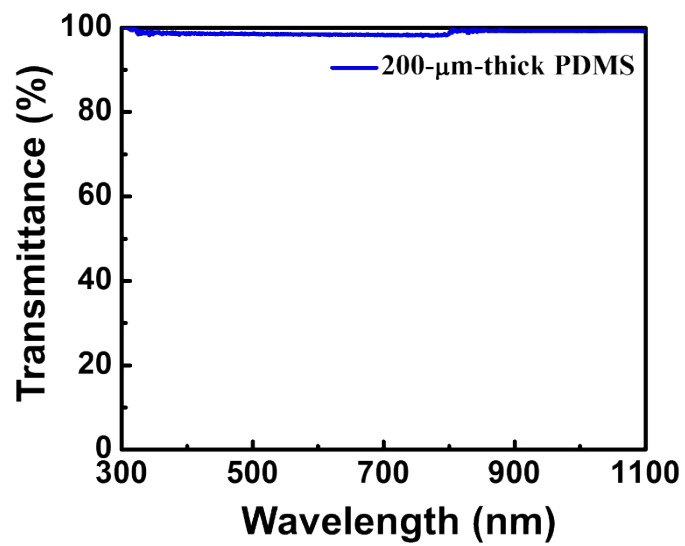


**Fig. S3.** Total transmittance spectrum of the 200  $\mu\text{m}$  thick PDMS film over the wavelengths 300–1100 nm.

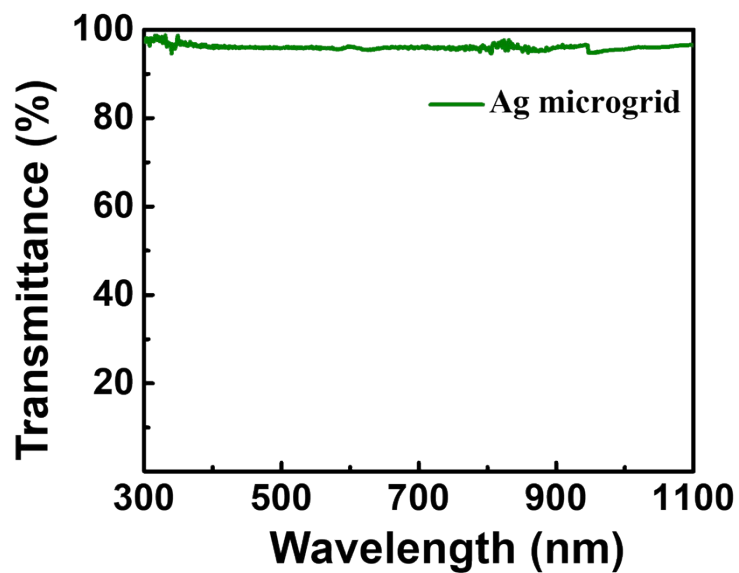


**Fig. S4.** Total transmittance spectrum of the Ag microgrid electrode embedded in PDMS film over the wavelengths 300–1100 nm.

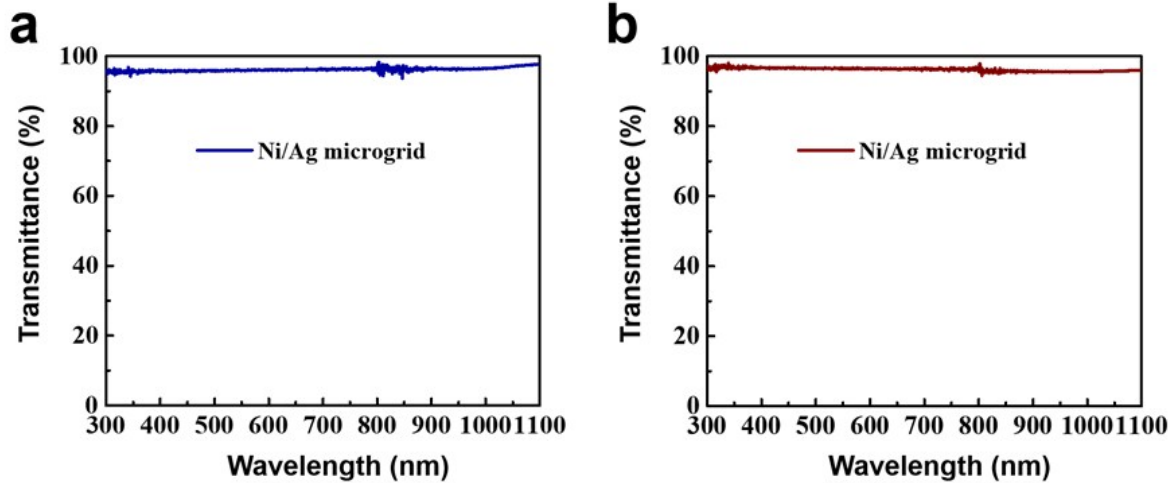


**Fig. S5.** (a) Total transmittance spectra referenced to air. (b) Total transmittance referenced to the substrate.

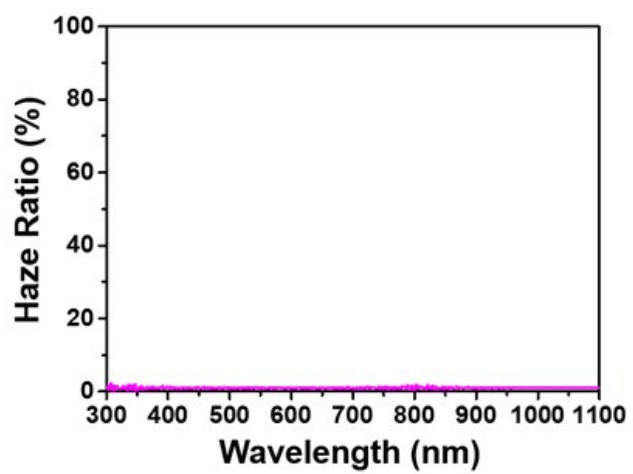


**Fig. S6.** (a) Haze ratio of the Ni/Ag hybrid microgrid electrode.



**Fig. S7.** SEM images of the AgNWs electrode (a) before oxidation and sulfurization and (b, c) after oxidation and sulfurization for 60 min, respectively.

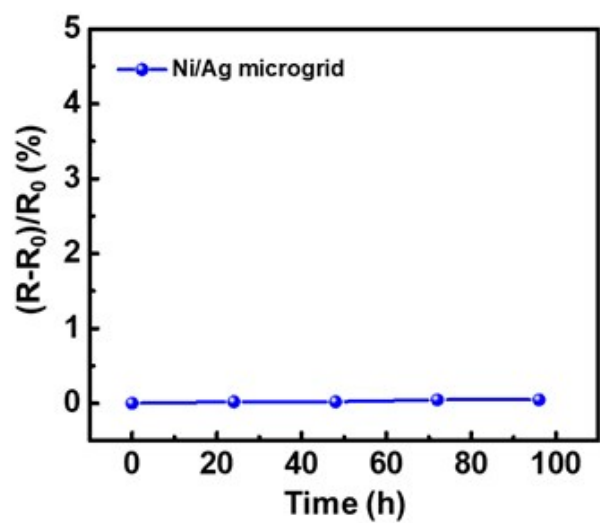


**Fig. S8.** Relative resistance as a function of time under 85% relative humidity and at 85°C for the Ni/Ag micro grid electrode.

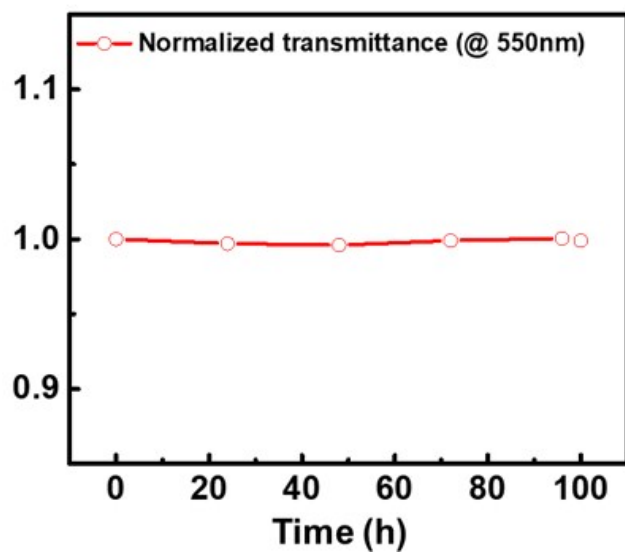


**Fig. S9.** Normalized transmittance of Ni/Ag microgrid electrode as functions of time under a real atmosphere (40% relative humidity and at 20°C).

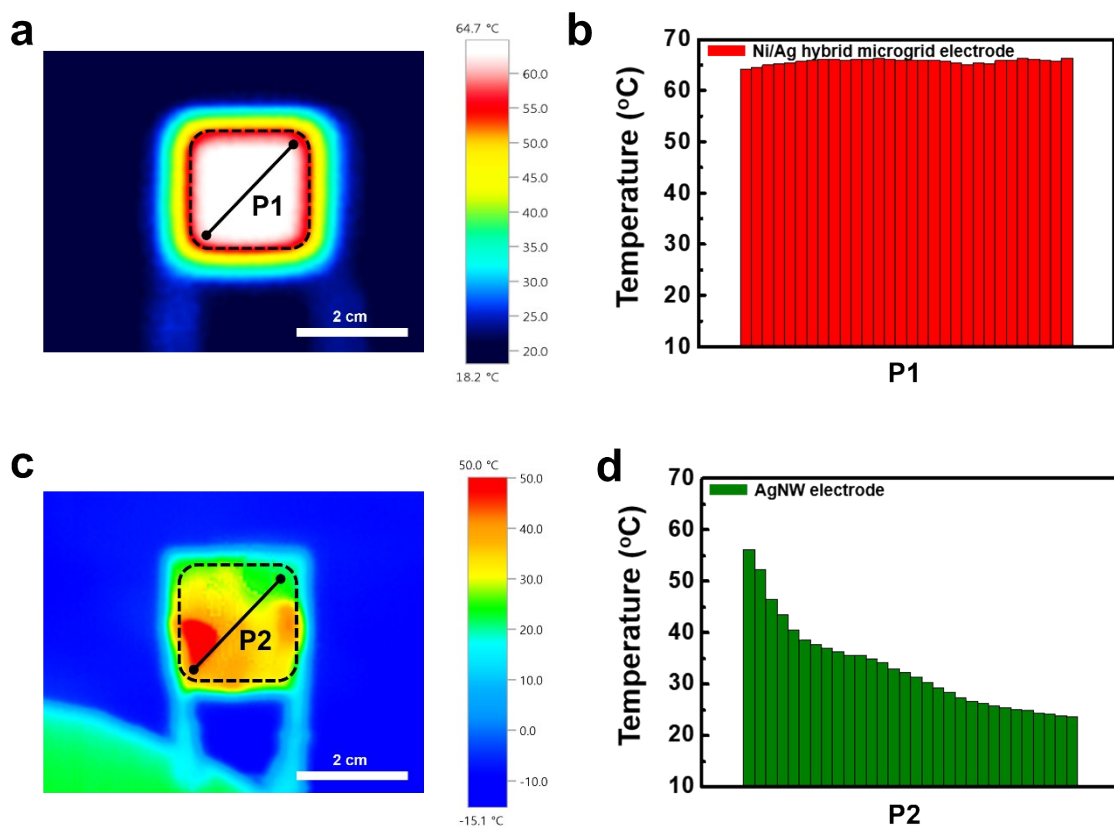


**Fig. S10.** (a) Infrared (IR) image of the Ni/Ag hybrid microgrid electrode-based transparent heater ( $20\text{ mm} \times 20\text{ mm}$ ) at an applied voltage of 3 V. (b) Histogram of temperature distribution in the Ni/Ag hybrid microgrid electrode-based transparent heater along the line labeled P1 in (a). (c) IR image of the AgNWs electrode-based transparent heater ( $20\text{ mm} \times 20\text{ mm}$ ) at an applied voltage of 3 V. (d) Histogram of temperature distribution in the AgNWs electrode-based transparent heater along the line labeled P2 in (c).

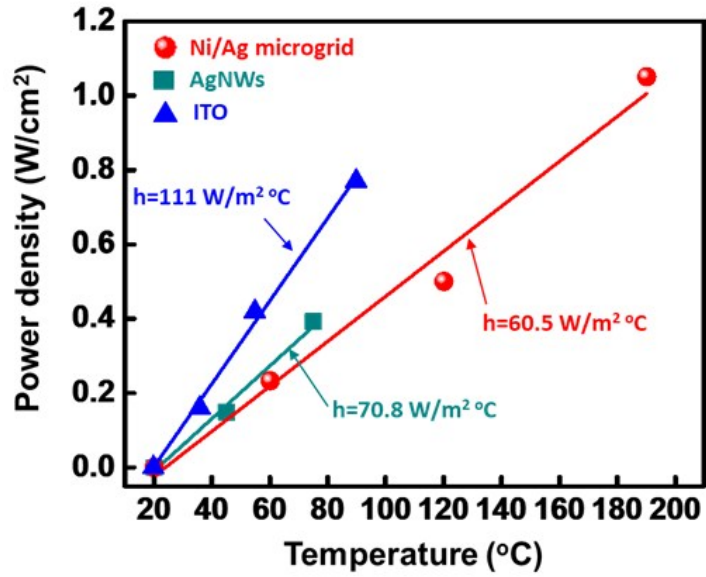
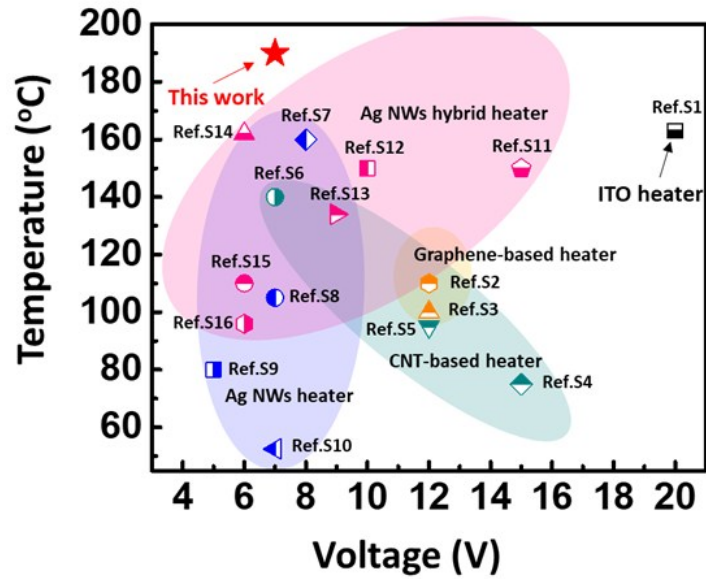


Fig. S11. Power density vs the saturated temperature of the Ni/Ag microgrid, AgNWs, and ITO.

Table. S1. Thermal equation parameters for the Ni/Ag hybrid microgrid, AgNWs, and ITO.

	<i>heat source flux</i> ( $q_{joules}$ $W/cm^2$ )	<i>temperature variation rate</i> ( $\Delta T/\Delta t$ , $^{\circ}C/sec$ )	<i>heat transfer coefficient</i> ( $h$ , $W/m^2$ $^{\circ}C$ )	$T_{ambient}$ ( $^{\circ}C$ )
Ni/Ag microgrid	0.5	2	60.5	20
AgNWs	0.393	0.79	70.8	20
ITO	0.419	0.47	111	20



**Fig. S12.** Comparison of saturated temperature of our Ni/Ag hybrid microgrid transparent heater with those of previously reported transparent heaters as function of an input voltage.<sup>1-16</sup>

**Table S2.** Summary of previously reported in transparent heaters.

material	Transmittance (% at 550 nm)	Input voltage (V)	Saturated temperature (°C)	Supporting Reference No. (Ref. S)
ITO	90	20	163	1
Graphene	92	12	110	2
	89	12	100	3
CNT	71	15	75	4
	79	12	95	5
	90	7	140	6
AgNWs	90	8	160	7
	90	7	105	8
	85	5	80	9
	90.5	7	52.5	10
AgNWs hybrid	90.2	15	150	11
	80	10	150	12
	86.4	9	134	13
	90	6	162	14
	82.8	6	110	15
	82.8	6	96	16
<b>This work</b>	<b>96</b>	<b>7</b>	<b>190</b>	

## Reference

1. K. Im, K. Cho, J. Kim and S. Kim, *Thin Solid Films*, 2010, **518**, 3960.
2. J. J. Bae, S. C. Lim, G. H. Han, Y. W. Jo, D. L. Doung, E. S. Kim, S. Chae, T. Q. Huy, N. V. Luan and Y. H. Lee. *Adv. Funct. Mater.*, 2013, **23**, 1250.
3. J. Kang, H. Kim, K. S. Kim, S.-K. Lee, S. Bae, J.-H. Ahn, Y.-J. Kim, J.-B. Choi and B. H. Hong, *Nano Lett.*, 2011, **11**, 5154.
4. H.-S. Jang, S. K. Jeon and S. H. Nahm, *Carbon*, 2011, **49**, 111.
5. Y. H. Yoon, J. W. Song, D. Kim, J. Kim, J. K. Park, S. K. Oh and C. S. Han, *Adv. Mater.*, 2007, **19**, 4284.
6. Y. Kim, H. R. Lee, T. Saito and Y. Nishi, *Appl. Phys. Lett.*, 2017, **110**, 153301.
7. J.-G. Lee, J.-H. Lee, S. An, D.-Y. Kim, T.-G. Kim, S. S. Al-Deyab, A. L. Yarin and S. S. Yoon, *J. Mater. Chem. A*, 2017, **5**, 6677.
8. T. Kim, Y. W. Kim, H. S. Lee, H. Kim, W. S. Yang and K. S. Suh, *Adv. Funct. Mater.*, 2013, **23**, 1250.
9. S. Hong, H. Lee, J. Lee, J. Kwon, S. Han, Y. D. Suh, H. Cho, J. Shin, J. Yeo and S. H. Ko, *Adv. Mater.*, 2015, **27**, 4744.
10. C. Celle, C. Mayousse, E. Moreau, H. Basti, A. Carella and J.-P. Simonato, *Nano Res.*, 2012, **5**, 427.
11. J. S. Woo, J. T. Han, S. Jung, J. I. Jang, H. Y. Kim, H. J. Jeong, S. Y. Jeong, K.-J. Baeg and G.-W. Lee *Sci. Rep*, 2014, **4**.
12. X. Zhang, X. Yan, J. Chen and J. Zhao, *Carbon*, 2014, **69**, 437.
13. J. Li, J. Liang, X. Jian, W. Hu, J. Li and Q. Pei, *Macromol. Mater. Eng.*, 2014, **299**, 1403–1409.
14. A.-Y. Kim, M. K. Kim, C. Hudaya, J. H. Park, D. Byun, J. C. Lim and J. K. Lee, *Nanoscale*, 2016, **8**, 3307.
15. S. Ji, W. He, K. Wang, Y. Ran and C. Ye, *Small*, 2014, **10**, 4951–4960.
16. Q. Huang, W. Shen, X. Fang, G. Chen, J. Guo, W. Xu, R. Tan and W. Song, *RSC Adv.*, 2015, **5**, 45836–45842